Spherical particles in small porous sphero-cylindrical systems: phase diagrams and transfer coefficients

Yu. K. Tovbin and D. V. Yeremich*

State Research Center of the Russian Federation "L. Ya. Karpov Institute of Physical Chemistry", 10 ul. Vorontsovo Pole, 105064 Moscow, Russian Federation. Fax: +7 (095) 975 2450. E-mail: tovbin@cc.nifhi.ac.ru

The equilibrium and transport characteristics of spherical particles in sphero-cylindrical porous systems were studied in terms of the lattice-gas model. The supramolecular structure of these systems is modeled by segments with a simple regular geometry (cylindrical and spherical) with additional inclusion of the interconnecting areas between different pore segments. Thus, one can model various types of porous systems ranging from zeolite cavities to stackings of long cylindrical sections in new mesoporous materials such as MCM-41 and MCM-49. The distribution of molecules is described in the quasichemical approximation with allowance for intermolecular interactions. The concentration dependences for local self-diffusion and shear viscosity coefficients were calculated. The contributions of the near-wall regions caused by the molecule—wall potential to the general pattern of phase diagrams, the effect of the pore size on the capillary condensation conditions, and the role of the molecular mobility on pore walls were discussed.

Key words: adsorbents, highly dispersed solids, adsorption isotherm, self-diffusion coefficient, shear viscosity coefficient, lattice-gas model, quasichemical approximation, argon, helium.

The phase states of the adsorbate in pores of different width are important characteristics of porous systems. The conditions for phase transitions with separation that gives rise to a two-phase state of the material adsorbed in narrow pores differ appreciably from the conditions of separation of macroscopic phases in the bulk phase. Analysis of the conditions of capillary condensation for pores with an ideal geometry (slit-like and cylindrical pores) showed that the pore wall potential influences the pattern of phase separation curves for a vapor—liquid system by changing the critical parameters (temperature of the condensation onset and the corresponding adsorbate density).[1—5] These critical parameters depend appreciably on the pore width and cross-section geometry. The conditions of adsorbate condensation are also affected by the nonuniformity of pore walls.[6] In turn, the phase distributions of the adsorbate, together with the structure of the porous system, influence the dynamic characteristics of the adsorbate.

Previously,[7] we formulated the changes in the description of equilibrium and kinetic characteristics needed to pass from individual pores to complex porous systems. These are due to the necessity of taking into account the following factors:

(1) limited length of a specific segment of a pore,

(2) the presence of transient segments (interconnections) between different neighboring pore segments,

(3) size (width and length) distribution of the pores in a macroscopic cross-section of a porous solid,

(4) type of stacking between pores of different type belonging to neighboring macroscopic cross-sections,

(5) changes in the type of local distribution of molecules over cross-sections of stackings and the conditions of capillary condensation of the fluid (critical temperatures and degrees of filling) in different segments of pore volume,

(6) the influence of the local structure of interconnections on the dynamic characteristics of the fluid, and

(7) orientation of the axis of a given pore segment relative to the direction of the macroscopic flux of molecules.

The first four factors determine the specific features of description of the pore space of complex porous systems, while the other refer to the description of the calculable equilibrium and dynamic characteristics of the adsorbate.

In this paper, we consider a simple example of porous system, namely sphero-cylindrical systems whose porous volume is formed by alternation of cylinders having a finite length and truncated spheres. These regular structures (Fig. 1, *a*) can model porous systems of various types. In particular, this refers to zeolite cavities,[8] which are approximated by spheres with relatively short cylindrical fragments of different diameters. The crossing of

Published in Russian in *Izvestiya Akademii Nauk. Seriya Khimicheskaya,* No. 11, pp. 2208—2219, November, 2003.

1066-5285/03/5211-2334 $25.00

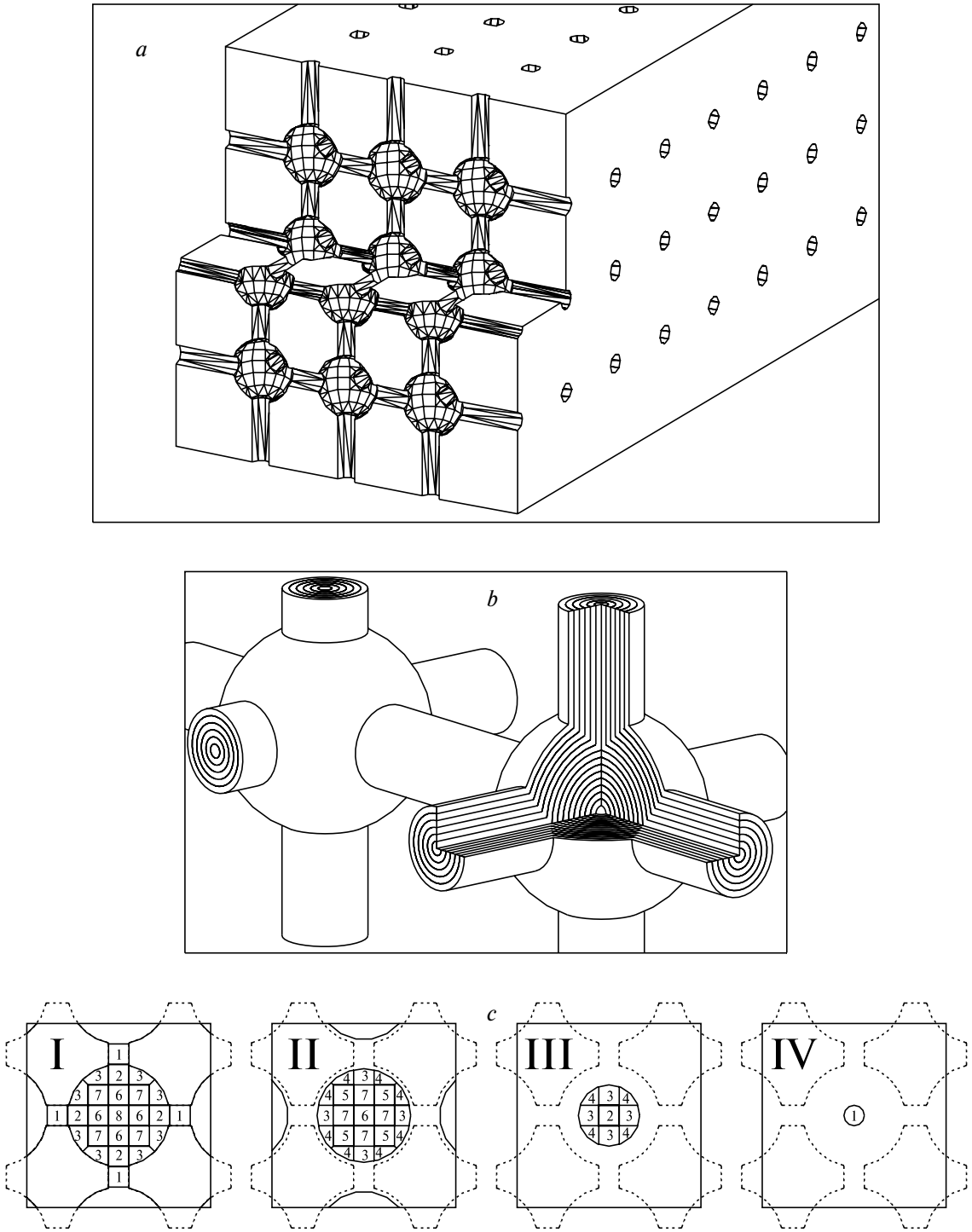

Fig. 1. Regular system of sphero-cylinders (*a*), separation of the pore volume into monolayers in sphero-cylinders (*b*) (the contour lines reflect the lattice molecular structure for the adsorbed molecules), and the lattice structure of adsorption sites: the distribution of sites in a "sphero-cylinder" consisting of a cylinder with site length with the diameter λ and a sphere with the diameter 5λ (*c*) (four cross-sections from the sphere center to the cylinder are shown, the continuous lines refer to the lines in plane I—IV, dashed lines, to the lines in plane I; the digits 1—8 designate sites with different adsorption properties).

long cylindrical segments in the FSM-16 materials and systems of disjoint cylinders in mesoporous materials, for example, MCM-41 and MCM-49 can also be modeled in this way.[9,10] (The interconnecting area of pores with different geometry in the neighborhood of the intersection line shown in Fig. 1, *a* is a transient area.)

A reported procedure[7] allows one to investigate the following properties of phase diagrams:

(1) the effect of the ratio of the sizes of the simplest pore segments on their contributions to phase diagrams,

(2) the contributions of the near-wall regions determined by the molecule—wall potential and the central parts of the pores to the phase diagrams, and

(3) the role and the length of transient regions.

Calculation of phase diagrams also makes it possible to follow the influence of capillary condensation on the concentration dependences of dynamic characteristics.

The lattice-gas model[11] can be used both to describe the structure of the porous system (supramolecular level) and to take into account the intermolecular interactions in the quasichemical approximation (molecular level). The calculation of the structure of a complex system is based on the procedure of isolation of model segments of a porous system with simple cylindrical and spherical shape and a system involving their intersections.[7,12]

At the molecular level, the lattice-gas model[11,13] takes into account the proper volume of the molecules and the interaction between them. This model ensures a self-consistent description of the equilibrium characteristics of a vapor—liquid system and the transfer coefficients of molecules in the bulk phase within the bounds of a quasichemical approximation with the use of a unified set of energetic model parameters. The model is applicable over broad ranges of fluid concentrations and temperatures. For narrow-pore systems, the model provides phase diagrams that are in good agreement with those obtained by molecular dynamics and Monte Carlo methods.[14,15]

Supramolecular level.[7,12] A real porous structure can be simulated by pore segments with the size $L > \lambda$, where λ is a linear dimension related to the diameter of the spherical adsorbate molecule. We will restrict ourselves to consideration of one supramolecular level, namely, the level of an adsorbent or catalyst pellet.[16,17] The scales L and λ correspond to the supramolecular and molecular levels, respectively. Let us specify the supramolecular structure by the distribution functions F_q and F_{qp}, which describe the fraction of type q segments and the probability that a type p segment is located near a type q segment, respectively;

$$\sum_p F_{qp} = F_q, \qquad \sum_p F_q = 1, \qquad 1 \le q, p \le M,$$

where M is the number of types of segments distinguished in a porous solid. The supramolecular level includes fragments of the porous body with a certain geometry (cylindrical and spherical) with the characteristic size D (for spheres and cylinders, D is the diameter). In the general case, $D \le L$. When $D = L$, a pore occupies the whole segment. When $D = 0$, no pore is present; hence, the neighboring segments are dead-end pores.

Let us also introduce the function H_{qp}, which is the conditional probability that a pore segment of type p is located near a pore segment of type q (along a chosen direction), $F_{qp} = F_q H_{qp}$ and $\sum_p H_{qp} = 1$. The function H_{qp} describes the connectivity of neighboring pore segments of different types at a supramolecular level. This allows one to compute the probabilities of existence of definite sequences of pore types by means of pair distribution functions, which are known analogs of pair functions used at the molecular level, in particular, analogs of the radial pair functions used in X-ray diffraction analysis (The function H_{qp} is the full analog of the functions $d_{fg}(1)$ (for designations, see Ref. 12), which apply to neighboring sites of a nonuniform system[12] and determine the conditional probability that a type g site is located near a type f site.)

Molecular level. According to the lattice-gas model,[11] the pore volume of segment q accessible for the adsorbate particles is subdivided into sites with the volume $v_0 = \lambda^3$ corresponding to the dimensions of the molecule ($\lambda = 1.12\sigma$, where σ is the molecular diameter). This rules out the possibility of double occupation of the cells (sites) by different molecules. The separation of sphero-cylindrical fragments into layers is shown in Fig. 1, *b*. Each layer is subdivided into elementary sites with the volume v_0, which form identical groups of sites. Figure 1, *c* shows the splitting of the space of regular sphero-cylinders consisting of a cylinder of site length with the radius $\lambda/2$ and a sphere with the diameter 5λ. Four nonrecurrent pore cross-sections (I—IV) of the seven cross-sections needed for representation of the total pore volume are shown. Cross-section I corresponds to the center of the cavity, while cross-section IV, to the cavity window. Numbers 1—8 in the Scheme designate sites with different adsorption properties.

In complex systems, the pore space of each segment q of the supramolecular structure is divided into the maximum number of molecules (N_q) that can be located inside the pore at complete filling. Generally, each site f ($1 \le f \le N_q$) of segment q can have its own probability of filling $\theta_{q,f}$ (the fraction of type f sites in a type q pore is designated by $F_{q,f}$). The site q,f can be characterized by the local Henry constant $a_{q,f} = a_{q,f}^0 \exp(\beta Q_{q,f})$, where $\beta = (kT)^{-1}$, T is temperature, k is the Boltzmann constant, $a_{q,f}^0$ is the preexponential factor, $Q_{q,f}$ is the binding energy of the molecule with pore walls, which includes the contributions of the walls located inside the radius of the adsorbate—adsorbent interaction potential. The isolation of fragment of an ideal structure with invariable $a_{q,f}$ values and interconnecting areas where $a_{q,f}$ values vary from one pore cross-section to another (for example, in pore cross-sections along the intersection of neighboring pores in Fig. 1, *a*) reduces substantially the set of site types $t(q)$ inside segment q. It is especially

important to take into account the symmetry properties of each pore segment.

In the case under consideration, one can write the following obvious relations generalizing similar expressions for the sites of a nonuniform lattice:[12]

$$F_{qp,fg}(r) = F_{q,f} H_{qp,fg}(r), \qquad \sum_{g=1}^{t(p)} H_{qp,fg}(r) = H_{qp},$$

where subscript g refers to a type p pore segment, $r \le R$, R is the radius of the interaction potential of molecules. If the functions $H_{qp,fg}(r)$ are constructed taking into account the variation of the properties of sites (adsorption sites) in the transient area, this generalization scheme of the lattice model would reflect not only the connectivity of pore segments of different types but also the features of their interconnecting areas, *i.e.*, it takes into account the structural defectiveness of the segments and nonuniformity of their walls. Evidently, these functions should obey the normalization relations

$$\sum_f F_{q,f} = F_q, \qquad 1 \le f \le t(q),$$
$$\sum_g H_{qp,fg}(r) = 1,$$
$$\sum_g F_{qp,fg}(r) = F_{q,f}$$

at any r. Within the segment q, each site f is characterized, under specified conditions, by local degrees of filling $\theta_{q,f}$ and the full ($\theta_{qp,fg}(r)$) and conditional ($t_{q,fg}(r) = \theta_{q,fg}(r)/\theta_{q,f}$, $\sum_g t_{q,fg}(r) = 1$) probabilities that adsorbate particles occupy neighboring sites f and g separated by the distance r. The number of sites of type g located at the distance r from site f is designated by $m_{qp,fg}(r)$, and the total number of sites in the coordination sphere of site f amounts to $z_{q,f}(r) = \sum_g m_{qp,fg}(r)$.

Local isotherms. Since each site is specified by two indices q and f, the adsorption isotherm $\theta(P)$ and the local degrees of filling of sites of different groups $\theta_{q,f}$ can be calculated using expressions obtained previously.[11] These expressions take into account the energetic nonuniformity of the lattice sites and the interactions between molecules A at a distance of R coordination spheres:

$$\theta(P) = \sum_q F_q \sum_{f=1}^{t(q)} F_{q,f} \theta_{q,f}(P),$$

$$a_{q,f} P = \theta_{q,f} \Lambda_{q,f} / (1 - \theta_{q,f}), \qquad (1)$$

$$\Lambda_{q,f} = \prod_r \prod_{p,g} \left[1 + x_{qp,fg}(r) t_{qp,fg}^{AA}(r)\right]^{d_{qp,fg}(r)},$$

$$x_{qp,fg}(r) = \exp[-\beta \varepsilon_{qp,fg}^{AA}(r)] - 1,$$

$$t_{qp,fg}^{AA}(r) = 2\theta_{p,g} / [\delta_{qp,fg}(r) + b_{qp,fg}(r)],$$

$$\delta_{qp,fg}(r) = 1 + x_{qp,fg}(r)(1 - \theta_{q,f} - \theta_{p,g}),$$

$$b_{qp,fg}(r) = [\delta_{qp,fg}(r)^2 + 4 x_{qp,fg}(r) \theta_{q,f} \theta_{p,g}]^{1/2},$$

where P is the adsorptive pressure, $\Lambda_{q,f}$ is the function taking into account the imperfection of the adsorption system in the quasichemical approximation, and $\varepsilon_{qp,fg}^{AA}(r)$ is the parameter of the lateral interaction of neighboring molecules at the distance r of the coordination sphere. This parameter may be a function of temperature and the local composition around sites q,f and p,g (the subscript g refers to a pore segment of type p). The subscripts p, g correspond to numbering of all neighbors $z_{q,f}(r)$ of the site q,f at distance $r \le R$ inside the pore; R is the radius of the interaction potential, $R < L$; $d_{qp,fg}(r) = z_{q,f}(r) H_{qp,fg}(r)$.

The following normalization relations are additionally taken into account

$$\theta_{qp,fg}^{AA}(r) + \theta_{qp,fg}^{Av}(r) = \theta_{q,f} \equiv \theta_{q,f}^{A},$$

$$\theta_{qp,fg}^{vA}(r) + \theta_{qp,fg}^{vv}(r) = \theta_{q,f}^{v} = 1 - \theta_{q,f},$$

$$\theta_{q,f}^{A} + \theta_{q,f}^{v} = 1,$$

where the superscript v implies vacancy, *i.e.*, a free site. The equilibrium distribution of particles over different types of sites θ_k can be found by solving the set of equations (1) by the Newton iteration method at specified value of θ. The accuracy of solution of this set is not less than 0.1%.

Calculation of phase diagrams. The densities of the coexisting vapor and liquid phases of the adsorbate were determined by the Maxwell construction.[11,13] Recall that all the first-order phase transitions are phase separation or condensation transitions (the term "phase separation" is more general) and the second-order phase transitions include ordering processes. Phase separation produces a two-phase state of low- and high-density substance. In complex adsorption fields, the nature of the surface potential stipulates directly the spatial domains in which the separation into the high- and low-density phases takes place. These spatial domains are manifested in different ways, depending on the nature of the surface potential and the coverage of the adsorbent. At some ratios of the molecule—pore wall and molecule—molecule interactions, these domains can be separated from each other. Under these conditions, the domains are filled successively upon an increase in the adsorptive pressure. For a one-component system composed of spherically symmetrical molecules (atoms), each spatial domain is described by a phase separation curve shaped like a dome and characterized by the critical density and temperature. (As usual, the phase diagrams are considered in the standard temperature—density (or concentration) coordinates.) In the case of narrow-pore systems, the liquid—vapor phase separation curves tend to have several

domes,[18,19] which are associated with coverage of surface layers and the remaining "central" part of the pore.

We will restrict ourselves to consideration of the immediate adsorbate—adsorbate neighbors ($R = 1$). The interaction energy is denoted by ε and it is assumed that $a_{q,f}^0 = 1$. The calculations were carried out for a lattice structure with $z = 6$, which corresponds to $(\beta\varepsilon)^{-1} = 1.234$ for the bulk phase. The phase diagrams were constructed in dimensionless coordinates, reduced temperature τ—dimensionless density of adsorbate θ, where $\tau = T/T_b$, T is temperature, and T_b is the critical temperature in the bulk phase. In these coordinates, the phase diagrams of all substances that obey the law of corresponding states have a universal form. As a rule, these substances are inert gases and some low-molecular-weight compounds.[18]

The interaction energy (Q) of the molecule with the surface will be represented as an integral taken over the solid space (Ω is the integration domain) for the specified atom—atom potential $U_{AS}(\rho)$ for interaction of the adsorbate (A) with atoms of the solid (S):

$$Q_{q,f} = \int_{\Omega} U_{AS}(\rho) n_S \mathrm{d}V,$$

$$U_{AS}(\rho) = 4\varepsilon_{AS}[(\sigma_{AS}/\rho)^{12} - (\sigma_{AS}/\rho)^6], \qquad (2)$$

where ρ is the distance from site f to volume element $\mathrm{d}V$ in the solid bulk; n_S is the density of distribution of the solid atoms in the adsorbent. For a flat adsorbent surface, relation (2) implies that the energy of binding of the adsorbate with the surface in the first monolayer $Q_1 = \alpha\varepsilon$; for the argon—carbon system, $\alpha = 9.24$,[18] while for adsorption of argon on silica gel, $\alpha = 3.9$.[19] The α values equal to 1.0 and 0 reflect the cases of weak attraction of the adsorbate by the wall (for polymeric sorbents) and the absence of adsorbate attraction by the wall. For the curved surfaces present inside cylindrical and spherical pores, the Q_1 values depend on the curvature: the smaller the radius, the greater Q_1. The relation $Q_2 = Q_1/8$, corresponding to the decrease in the attraction in proportion to f^{-3}, where f is the number of the monolayer counted off from the pore wall, is retained qualitatively for sites in the second monolayer. The pore sites with equal Q values belong to the same type. All the internal sites separated from the pore walls by distances such that the Q value is ~1/20 of the mean kinetic energy of the adsorbate or smaller were classified as central sites of the pore with $Q_{f>2} = 0$.[18]

Let us express the diameters of cylindrical and spherical segments in terms of the linear dimension of site λ. The regular structure of sphero-cylinders will be designated as D_s—D_c—L_c, where D_s is the sphere diameter, D_c is the cylinder diameter, and L_c is the length of the cylindrical channel. Below we consider the cases of discrete variation of these values.

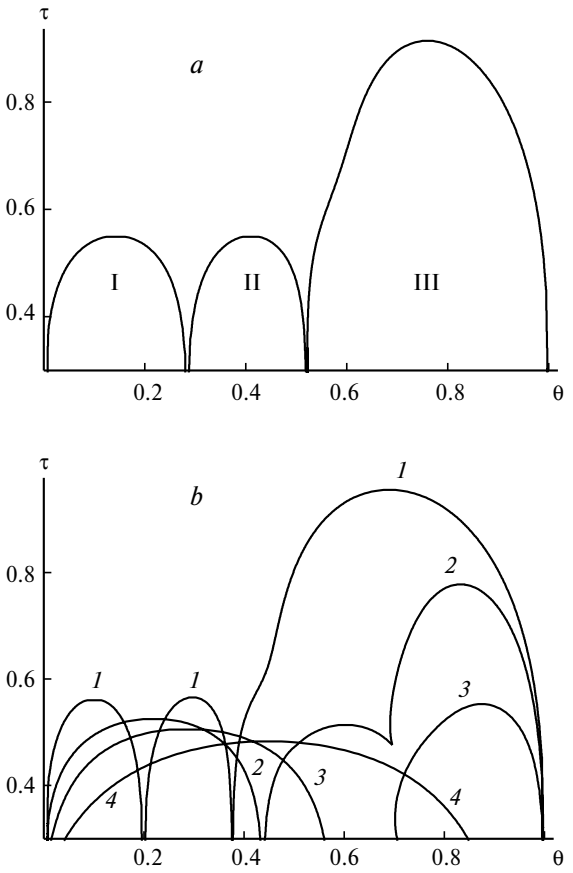

Fig. 2. Full phase diagram with separation for a cylindrical pore with $D_c = 8$ (*a*) (I—III are the numbers of domes) and phase diagrams for isolated cylindrical pores (*b*) with $D_c = 19$ (*1*), 13 (*2*), 5 (*3*), 3 (*4*).

Cylindrical systems. Phase diagrams of the Ar—SiO_2 system obtained for the condensation of Ar atoms in isolated pores of different diameters in SiO_2-based materials are shown in Fig. 2 (more precisely, five monodisperse pore systems are considered). The complete phase diagram with phase separation for a cylindrical pore (see Fig. 2, *a*) consists of three domes (they are numbered in the order of increasing θ): domes I and II correspond to sites located in the first and second surface monolayers, respectively, while dome III corresponds to filling of the remaining central (or bulk) part of the pore. This dome describing the adsorbate condensation in the central part of the pore is considered in most publications (see Ref. 20). The width of each dome is proportional to the fraction of sites of the given type. Figure 2, *b* shows the variation of the form of the full phase diagram following the change in the diameter D_c of the cylindrical pore. In the case of the cylinder with the largest diameter the phase diagram also consists of three domes (curve *1*). A decrease in the cylinder diameter gives rise first to three incompletely resolved domes (curve *2*), then to two domes (curve *3*),

and, finally, for the smallest diameter equal to three adsorbate monolayers, the diagram is represented by one dome (curve *4*).

For relatively wide cylinders (see Fig. 2, *a* and Fig. 2, *b*, curve *1*), each complete phase diagram with separation consists of three domes. The wider the pore, the higher the critical temperature and the lower the critical density of the third dome. As the pore size increases, the area of coverages corresponding to the formation of surface layers decreases; hence, the width of the first two domes decreases. It is noteworthy that the heights of both surface domes are virtually the same, which is due to the two-dimensional character of condensation in both surface layers.

A decrease in the diameter of a cylindrical pore entails a decrease in the critical temperature (see Fig. 2, *b*). This fact is well-known for domes that are associated with the central part of the pores.[1—6,20] However, it is also valid for the surface domes. Whereas the decrease in the critical temperature for the domes of the central part of the pores is due to the size effect, in the case of surface domes this is due to an increase in the adsorbate—adsobent binding energy, because the wall curvature becomes more pronounced with a decrease in the diameter. The critical temperatures in the surface layers are similar (see Fig. 2, *b*, curves *1* and *2*) but differ appreciably from the critical temperature for the dome describing the filling of the central part of the pore. This feature is due to the maintenance of the two-dimensional character of condensation on the curved surface layers of a cylindrical pore up to disappearance of the third dome.

Complete phase diagrams for a polydisperse system of isolated pores with the diameters $D_c = 8, 9, 10$, and 11 are shown in Fig. 3. In the case of a uniform pore size distribution function (see Fig. 3, *a*, *b*), the distribution function has the form $F_q = 1/M$. (The main properties of full phase diagrams were considered for a system of cylindrical pores consisting of four pores ($M = 4$) with different

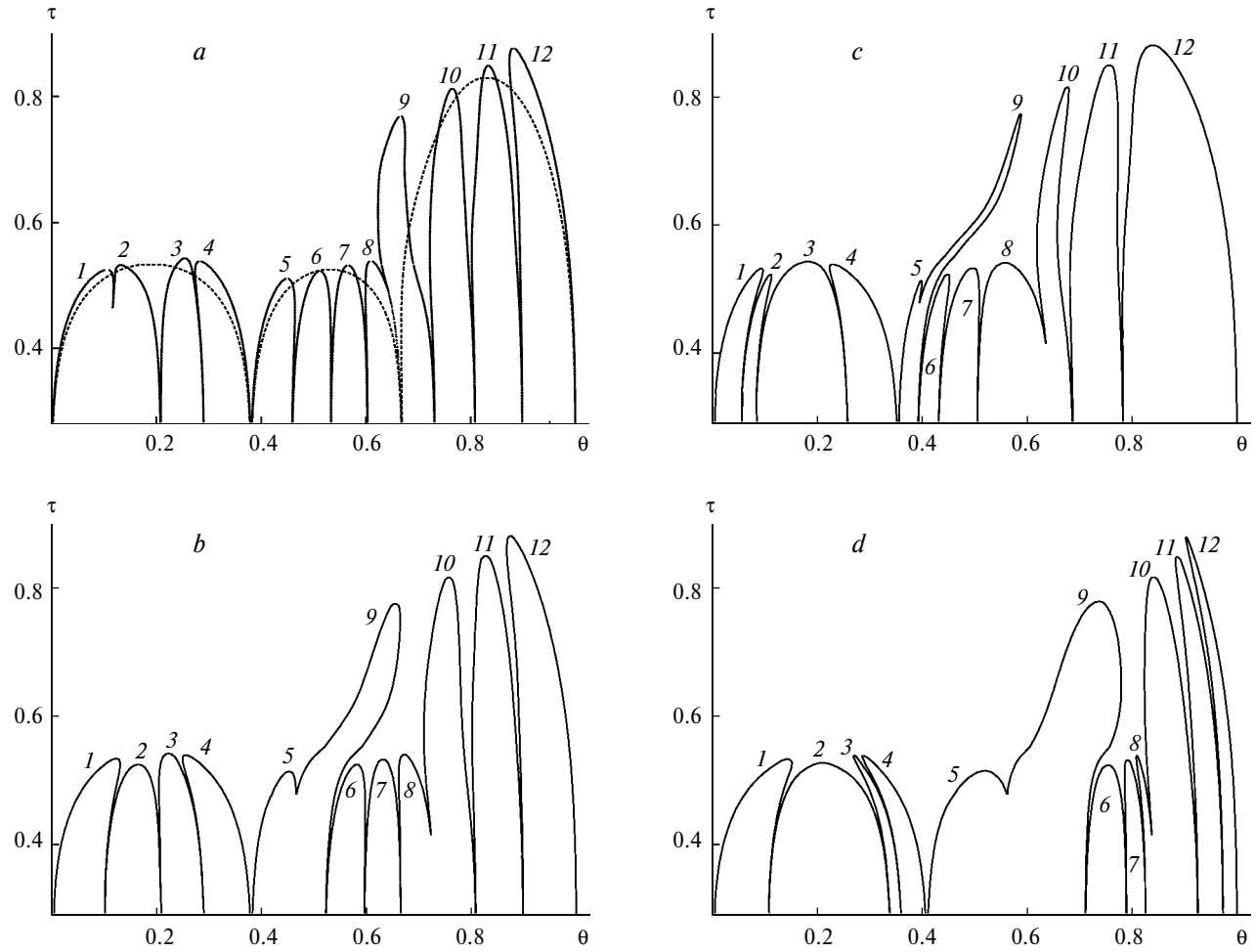

Fig. 3. Phase diagrams for porous systems of the Ar—C (*a*) and Ar—SiO_2 (*b*—*d*) types consisting of four isolated cylinders with the diameters $D_c = 8, 9, 10$, and 11. The pore size distribution functions: smooth (*a*, *b*), ascending (*c*), and descending (*d*). The dashed line in Fig. 3, *a* corresponds to the diagram constructed without taking into account the effect of pore size on the condensation conditions in the surface and central layers. The digits correspond to the numbers of domes (see explanation in the text).

widths; for $M > 4$, the size of the figure should have been increased). For a system of isolated infinitely long pores, the function $H_{qp} = \Delta_{qp}$ (Δ_{qp} is the Kronecker delta-function). To take into account the limitedness of the length of pore segments and the modes of their interconnection, detailed description of the mutual arrangement of sites of different types is required (see Fig. 1, *c*).

For a highly attractive adsorbent—adsorbate potential, the complete phase diagram (see Fig. 3, *a*) consists of 12 domes, three domes being realized for each of the four pores. Domes *1—4* refer to the surface layers of pores of different widths, while domes *5—8* correspond to the second surface layers in different pores. Due to different curvatures of the walls, the adsorbent—adsorbate binding energy is different in all pores; therefore all the surface domes are split. Domes *9—12* refer to filling of the central regions of various pores. For these, splitting is due to the difference between the pore diameters (size effect) because the adsorbent—adsorbate binding energy is much lower than the adsorbate—adsorbate binding energy.

For visual illustration of the effect of dome splitting under the action of the surface potential, Fig. 3, *a* was supplemented by a "simplified" phase diagram (with three domes) calculated assuming that the binding energies are the same in each of the two surface layers for any diameter and that the degree of filling for the central regions of the four pores considered is the same. With these two conditions, the phase diagram of the system resembles the phase diagram for an individual pore shown in Fig. 2. In particular, there are differences in the second surface and central domes but, no specifics for pores with different diameters. In this case, the critical parameters of the domes for the given system of pores are the weighted average values of the corresponding values for individual pores, while the widths of the three domes of the "simplified" phase diagram coincide with the overall widths for domes *1—4*, *5—8*, and *9—12*, respectively, on the initial phase diagram. Thus, taking into account the specific character of each pore determined by the pore diameter results in splitting of each of three domes of the "simplified" system into individual contributions of M pores ($M = 4$).

The effect of the adsorbent—adsorbate potential on the form of the complete phase diagram can be seen by comparing Fig. 3, *a* and 3, *b*. The transition from the system with $\alpha = 9.24$ to a system with $\alpha = 3.9$ characterized by weaker interaction of the adsorbate with the wall (see Fig. 3, *b*) entails a substantial shift of the position of the central dome for the narrowest pore (dome *9* in Fig. 3, *a*) to the region corresponding to filling of the second layers: the central dome for $D_c = 8$ is located near the dome for the second layer of this pore (between domes *5* and *6*). The domes for the second layers in pores with $D_c > 8$ (domes *6—8*) appear at higher fillings than dome *9*. One more specific feature of the diagram in Fig. 3, *b* is associated with the change in the upper segments of the domes for the surface layer caused by a change in the surface potential.

A marked difference between the domes shown in Fig. 3, *a*, *b* and those in Fig. 2 lies in a more clearly defined curvature, *i.e.*, in the position of the critical points with respect to the midpoint of the dome width at relatively low temperatures (where the dome boundaries are nearly vertical). Whereas for the domes shown in Fig. 2, the critical densities occur near the dome centers, in the case of Fig. 3, *a*, *b*, one can see that the critical densities can not only shift to either right or left end of the dome section but can also occur beyond this dome section (the dome width). The nature of this effect is related to simultaneous filling of pores with different widths in different proportions on a change in the external pressure of the adsorptive. If different pores were filled simultaneously, the shape of individual domes in Fig 3 would not change either, as in Fig. 2. Only the width of domes would change in conformity with the fraction of the given pore F_q. The change in the dome shape attests to simultaneous filling of different pores. In the case of a polydisperse system composed of M isolated pores, a complete phase diagram can be obtained by mere addition of the phase diagrams of separate pores (as in Fig. 2) taking into account the degree of filling of each pore for the current adsorptive pressure and their fraction F_q in the porous system. (This allows one to solve the set of equations (1) only for individual pores and then to take into account their fractions and not to solve the same set of equations of a much greater dimensionality for the whole porous system.)

The role of the pore size distribution function F_q is illustrated by Figs. 3, *b—d*. Figure 3, *c* shows the phase diagram with an exponentially increasing pore size distribution function

$$F_q = \exp(Aq)/\sum_{q=1}^{4}\exp(Aq),$$

where $A > 0$ is a constant. Here it is assumed that $F_1/F_4 = 0.066/0.536$. Figure 3, *d* shows the phase diagram with an exponentially decreasing ($A < 0$) pore size distribution function ($F_1/F_4 = 0.536/0.066$). The order of arrangement of all domes does not change with a change in F_q.

The widths of all second surface and central domes in Fig. 3, *b—d* is well correlated with the pore fraction F_q. Meanwhile, the width of each of the first four surface domes is determined not only by F_q but also by $F_{q,1}$ of the surface sites, which change most appreciably upon the change in the diameter of cylindrical pores. As a result, dome *3* (rather than *4*) is the widest one in Fig. 3, *c*, while dome *2* (rather than *1*) is the widest one in Fig. 3, *d*. Thus, even for a system of isolated pores, the form of the complete phase diagram depends on both the pore size distri-

bution function and the contribution of particular type of sites in each pore.

Intersecting cylindrical pores. The intersection of channels results in a change in the adsorption properties of the walls near the intersection areas; a part of the volume of the solid is occupied by a neighboring pore that intersects the given pore and, therefore, the adsorbent—adsorbate binding energy decreases. By changing the length of the cylindrical segment of the pore L_c, one can substantially change the energy characteristics of the adsorbent—adsorbate system; for $L_c \to \infty$, we have isolated channels. The condition of intersection of cylindrical channels is described by the relation $D_s = D_c$. We studied a three-dimensional structure with six channels outgoing from each crossing point.

The phase diagrams for regular three-dimensional structures composed of intersecting cylindrical channels are shown in Fig. 4. Narrow (Fig. 4, *a*) and wide (Fig. 4, *b*) microporous systems are presented. For narrow channels (see Fig. 4, *a*), the surface sites account for the main portion of all sites; therefore, their domes are wide; curve *1* correspond to the case where the channel length and width are equal to each other. This results in a sharp decrease in the adsorbent—adsorbate binding energy; therefore, the dome that refers to the surface sites is characterized by the highest critical temperature. An increase in the channel length L_c induces an increase in the adsorbent—adsorbate binding energy and a decrease in the critical temperature of the surface dome (curve *2*). For curve *3*, the channel length is markedly greater than its width; this corresponds to the highest adsorbate—adsorbent binding energy. In this case, the critical temperature for a surface dome corresponding to sites inside the channel becomes lower than the critical temperature for the weakest adsorption sites in the intersection area. The same type of curves is presented in the diagrams in Fig. 2; however, in Fig. 4, *a*, the critical temperatures for all domes are much lower due to the small pore size. The geometric parameters of curve *2* correspond to the He—silicalite system for which D_s—D_c—L_c = 2—2—4.[8] For the Ar—paulingite system, the parameters D_s—D_c—L_c = 1—1—3 [8] are also close to those of the curves shown in Fig. 4, *a*.

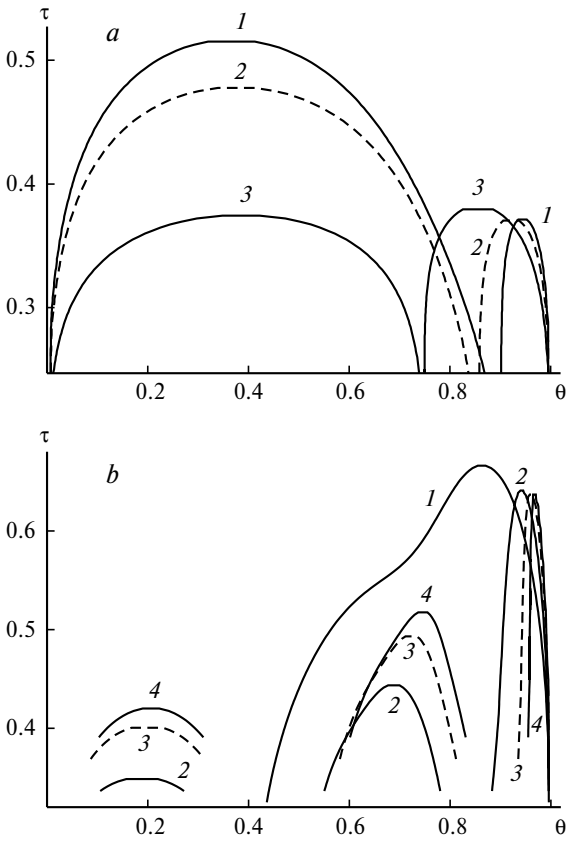

Fig. 4. Phase diagrams for three-dimensional systems of intersecting cylinders with the parameters $D_s = D_c = 2$, $L_c = 2$ (*1*), 4 (*2*), 6 (*3*) (*a*) and $D_s = D_c = 5$, $L_c = 1$ (*1*), 5 (*2*), 10 (*3*) 15 (*4*) (*b*).

For wider channels (see Fig. 4, *b*), characteristics of the surface domes change only slightly (curves *2—4*). (For curve *1*, this dome corresponds to $\tau < 0.32$; however, it should be noted that this curve refers to site length of the channel, resulting in a very open structure with exceptionally specific properties, in particular, with a relatively low mechanical strength.) The critical temperatures for second surface domes corresponding to sites near channel intersections substantially increase. Finally, apart from the two domes corresponding to filling of different sites in the channels, the third surface channels (curves *2—4*) corresponding to regions with the weakest adsorbate—adsorbent potential also appear. Comparison with the phase diagram for isolated cylinders (see Fig. 2, curves *3* and *4*) indicates that the presence of intersections of cylindrical channels changes the number of domes. Thus, the effects of pore intersection can mask the properties of a porous system; three completely separated domes are observed in the case of isolated pores for $D_c > 8$ (in Fig. 4, *b* D_c = 5!) and the properties of the domes (the shape, width, and critical parameters) are appreciably different.

Regular structures of sphero-cylindrical pores. The presence of truncated spheres in the intersection area of cylindrical channels gives rise to wider sections of the porous system. Curves *1—3* in Fig. 5 correspond to systems with increasing diameter of the spherical segments with constant dimensions of the cylindrical segments. With an increase in D_s, the height of the dome corresponding to the intersection area of the cylindrical and spherical pores increases. These curves can be regarded as analogs of the third domes present in Fig. 4, *b*. In this case, the contributions of the intersection areas predominate over the contributions of the near-wall areas (the missing surface domes correspond to lower temperatures and degrees of filling). Therefore, the width of the domes that describe filling of the second layers decreases when the critical

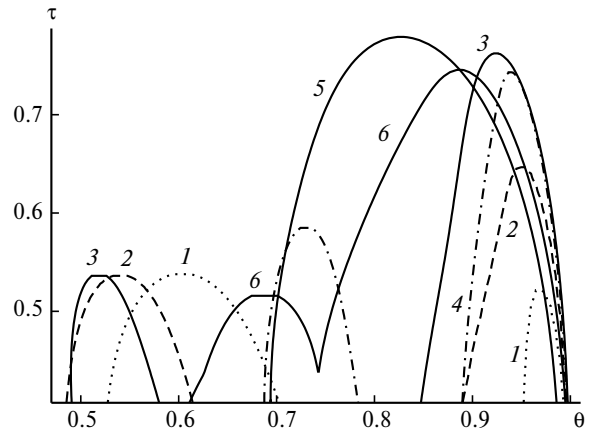

Fig. 5. Phase diagrams for regular sphero-cylindrical structures with the parameters D_s—D_c—L_c = 6—4—8 (*1*), 8—4—8 (*2*), 10—4—8 (*3*), 9—6—8 (*4*), 9—8—8 (*5*), and 9—6—1 (*6*).

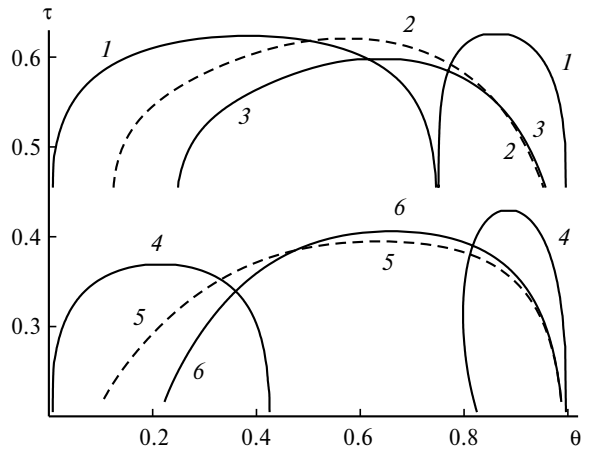

Fig. 6. Phase diagrams for regular microporous sphero-cylindrical structures with the parameters D_s—D_c—L_c = 3—2—2 (*1*), 3—1—1 (*2*), 3—1—2 (*3*), 4—2—2 (*4*), 4—1—1 (*5*), and 4—1—2 (*6*); curves *1*—*3* are shifted to greater τ values by 0.25.

temperature is invariable, and the critical temperatures of the third domes increase with an increase in D_s.

Curves *4* and *5* illustrate the influence of an increase in the diameter of the cylindrical channel for $L_c = 8$. Both domes (see Fig. 5) correspond to cylinder segments in the vicinity of intersection with a sphere and to the common central part for both types of pores. For these, an increase in the diameter D_c entails an increase in the critical temperatures.

A decrease in the length of the cylindrical channel (curves *4* and *6*) results in virtual degeneration of the surface sites inside the channels. The critical temperatures for central sections of spherical pores do not change, while the proportion of these sections considerably increases. The structure with D_s—D_c—L_c = 9—6—1 for curve *6* is highly open; this appreciably decreases the adsorbate—adsorbent binding energy and the mechanical stability of the adsorbent.

The microporous sphero-cylinders typically have small D_s—D_c—L_c values. Correspondingly, the total internal volume of the pores is in the range of the surface potential fields characterized by high energies (see Eq. (2)). As a result, the critical temperatures of all domes significantly decrease. Comparison of the curves in Fig. 6 with those in previous Figures shows that the curves in Fig. 6 resemble the domes of surface layers. Based on geometric parameters, the calculations presented in Fig. 6 correspond to the following zeolite systems: D_s—D_c—L_c = 3—1—1 (Ar—chabazite and Ar—levynite with two windows instead of six), 4—1—1 (Ar—zeolite A and He—zeolite A).[8] The Ar—zeolite X (12 windows), 3—2—1, and He—chabazite, 4—2—1, systems also fall within the considered region of geometric parameters[8]

By comparing curves *1* and *4* (or *2* and *5*, or *3* and *6*) in Fig. 6, one can follow the effect of an increase in the sphere diameter. The sharp decrease in the width of the first dome for curve *4* is due to a decrease in the proportion of sites of the cylindrical part induced by an increase in D_s. A strong nonuniformity of sites in the transient region of a sphero-cylindrical pore results in the fact that no separate dome is formed upon filling of these sites in the given temperature region; therefore, the dome width for the spherical part does not increase, although the critical temperature increases. However, filling of sites in the transient region influences the curvature of this dome. Curves *1* and *3* (and *4* and *6*) reflect the effect of an increase in the diameter of a cylindrical channel on the form of the phase diagram, while curves *2* and *3* (and also *5* and *6*) reflect the effect of an increase in its length. The general trends in the variation of the properties of phase diagrams depending on the geometric parameters of the structure are similar to those mentioned above for systems with wider pores (see Fig. 5).

However, it is noteworthy that under real external conditions, for example, for Ar atoms at $\tau \leq 0.5$, the substance occurs in the solid or supercooled liquid state.[21] An increase in the wall potential induces a decrease in the critical temperature of condensation, but its influence on the melting conditions has not yet been identified for certain. As shown previously,[22,23] an increase in the attractive potential of the walls decreases both the melting point and the critical condensation temperature. Data indicating the possibility of increasing the melting point, which results in sharp reduction of the coexistence region of the two-phase liquid—vapor system, have been reported.[20] Equation (1) does not reflect the possibility for the fluid to pass in the solid state and does not describe the two-phase melting region (liquid—solid). Therefore, the agreement of calculations for microporous sphero-cylinders (see Fig. 6) and real zeolite systems is, apparently, restricted to the temperature region $\tau > 0.30$—0.35.

The obtained results of calculations of the critical temperatures and densities attest to a substantial influence of the characteristic pore volume on the conditions of adsorbate separation. The presence of the surface attractive potential creates conditions for filling of the first two or three surface layers on pore walls. If the volumes of these layers are subtracted from the pore volume, the remaining space can conventionally be considered uniform. Its filling is related to the usual capillary condensation where two-phase states arise within the pore ensemble. As the pore size decreases, the reduced temperature τ decreases to ~0.5 or lower. This means that a two-phase state can be attained upon a substantial decrease in the system temperature. Nitrogen is used most often to estimate the system porosity. Its critical temperature equals ~126 K.[21] The obtained range $\tau = 0.3—0.5$ is matched by temperatures of ~38—63 K. It is known that such low temperatures are not employed in conventional adsorption measurements; therefore, naturally, phase transformations do not take place in real microporous systems and the model we considered properly reflects the physical phenomena. In addition, this model can be used to estimate what temperature drop is needed to observe phase separation effects in microporous systems. It is clear that at these low temperatures, equilibration may be highly retarded due to diffusion.

Local dynamic characteristics. The simultaneous action of the adsorption potential of the pore walls and the intermolecular interaction results in equilibrium distributions of molecules being highly nonuniform over pore cross-sections. In calculation of any dynamic coefficients, it is assumed that the equilibrium distributions of molecules change slightly; therefore, they are found using equations like (1). The self-diffusion and shear viscosity coefficients are the most important characteristics used to describe fluxes of molecules of one sort.

The local self-diffusion coefficient (D^*) describes redistribution of molecules among neighboring sites. It is calculated from the expression[24]

$$D^*_{qp,fg}(\rho) = \rho^2 z^*_{qp,fg} U_{qp,fg}(\rho)/\theta_{q,f}, \qquad (3)$$

where $z^*_{qp,fg}$ is the number of possible jumps from site q,f into site p,g by the distance ρ; $U_{qp,fg}(\rho) = K_{qp,fg}(\rho)V_{qp,fg}(\rho)$ is the flux (the rate of molecule jumps per site time) from site f to site g by distance ρ, which describes the velocity of migration of molecules along the given direction; $K_{qp,fg}(\rho)$ is the rate constant for jumps, $K_{qp,fg}(\rho) = K^0_{qp,fg}(\rho)\exp[-\beta E_{qp,fg}(\rho)]$, $E_{qp,fg}(\rho)$ is the activation energy for a jump, $K^0_{qp,fg}(\rho)$ is the pre-exponential factor, $V_{qp,fg}(\rho)$ is the concentration component of the rate of jumps (depends on the ratio of the interactions of a molecule in the ground ($\varepsilon^{AA}(r)$) and transition ($\varepsilon^*(r) = \alpha\varepsilon^{AA}(r)$) states). The expressions $U_{qp,fg}(\rho)$ were derived using the theory of absolute reaction rates in condensed phases.[11,24,25] The constants for jumps and the local Henry constants are related as follows: $a_{q,f}K_{qp,fg}(\rho) = a_{p,g}K_{pq,gf}(\rho)$. The values used in calculations were $\alpha = 0.5$ and $\alpha_{11} = E_{11}/Q_1 = 0.3$, where E_{11} is the activation energy for the molecular jump along the pore wall, $\rho = 1$.

The concentration dependences of the self-diffusion coefficients for crossing microchannels and a mesoporous sphero-cylindrical systems at different temperatures are shown in Fig. 7. The curves are normalized to the corresponding self-diffusion coefficients for small densities of the bulk phase at a fixed temperature (D_b^*). This is the reason for different self-diffusion coefficients for zero den-

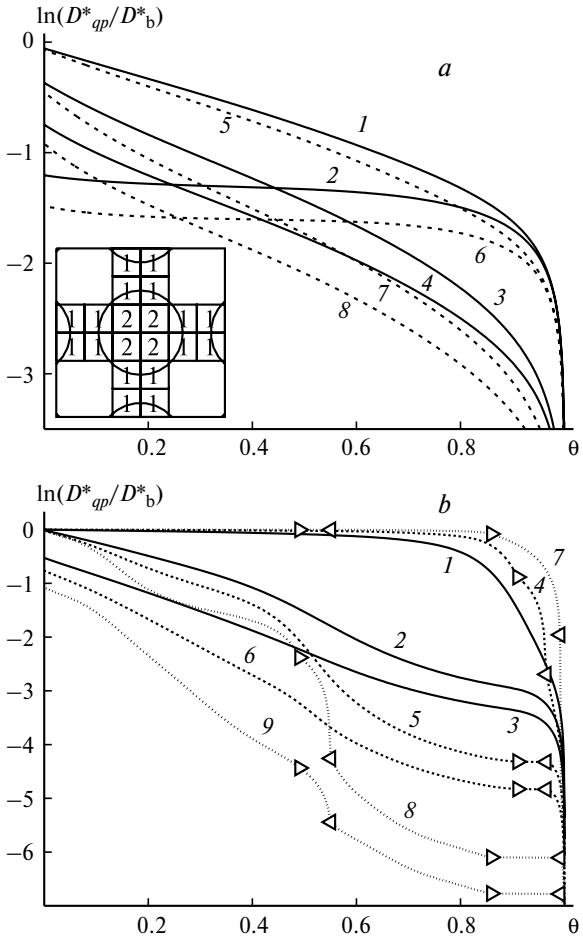

Fig. 7. Concentration dependences of self-diffusion coefficients (D^*) for intersecting microchannels with $D_s—D_c—L_c$ = 2—2—2 (*a*) and for a mesoporous sphero-cylindrical structure with $D_s—D_c—L_c$ = 10—4—8 (*b*): (*a*) $(\beta\varepsilon)^{-1}$ = 1.23 (*1—4*), 1.00 (*5—8*); the following values are given: $D^*_{1,1}$ (*4*, *8*), $D^*_{1,2}$ (*2*, *6*), $D^*_{2,1}$ (*1*, *5*), $D^*_{2,2}$ (*3*, *7*); (*b*) $(\beta\varepsilon)^{-1}$ = 1.23 (*1—3*), 0.85 (*4—6*), 0.60 (*7—9*); the following values are given: $D^*_{1,1}$ (*3*, *6*, *9*), $D^*_{11,11}$ (*2*, *5*, *8*), $D^*_{23,23}$ (*1*, *4*, *7*). The characters "▷" and "◁" designate the two-phase regions. The inset in Fig. 7, *a* reflects the positions of type 1 sites in the channel and type 2 sites in the intersection area and the difference between their adsorption properties due to energy differences (see Eq. (2)).

sities. Figure 7, *a* shows the local self-diffusion coefficients for molecules in a channel (pairs of sites 11, inside the channel; and 12, from the channel to the intersection area (see the inset)) and for two directions of the molecular motion in the intersection area (pairs of sites 21, from the intersection area to the channel and 22, between the sites of the intersection area) calculated for $(\beta\varepsilon)^{-1} = 1.23$ and 1.00. The temperature dependence for jumps in the intersection area is least pronounced. For migration along a cylindrical channel, the temperature dependence is most pronounced due to the high activation energy for surface migration.

The concentration dependences of the self-diffusion coefficients in a regular sphero-cylindrical system at three temperatures corresponding to $(\beta\varepsilon)^{-1} = 1.23$, 0.85, and 0.60 are shown in Fig. 7, *b*. Curves *1—3* refer to the supercritical region, curves *4—6*, to the temperature corresponding to condensation in the central part of the system for degrees of filling of $\theta \approx 0.90$—0.96, and curves *7—9*, to the temperature where two domes are formed, one for the sites located in the second surface region ($\theta \approx 0.5$) and the central region ($\theta = 0.86$—0.98). The patterns of the curves in the regions of capillary condensation were calculated taking into account the Maxwell rule (lever relation). Two-phase regions are placed between characters "$\triangleright$" and "$\triangleleft$" in these curves. Curves *4—6* have one two-phase region, while curves *7—9*, two such regions. (The numbers of site pairs correspond to the following regions: 11, surface sites in a cylinder (curves *3*, *6*, *9*); 11,11, central sites in a cylinder (curves *2*, *5*, *8*); and 23, 23, the central sites in a sphere (curves *1*, *4*, *7*).) The results of calculations demonstrate strong influence of the surface potential and temperature on the thermal migration of molecules. Upon a decrease in the temperature, the role of capillary condensation is enhanced.

Within the framework of the generalized Eyring model,[26] the expression for the local shear viscosity coefficient for the shear of a fluid in site *g* relative to site *f* by distance ρ has the form

$$\eta_{qp,fg}(\rho) = \eta_0 \exp[\beta E_{qp,fg}(\rho)]/V_{qp,fg}(\rho), \qquad (4)$$

where $\eta_0 = (mkT/\pi)^{1/2}/(\pi\sigma^2)$ is the viscosity of an ideal rarefied gas, *m* is the atom mass, σ is the diameter of the molecule, $E_{qp,fg}(\rho)$ is the activation energy for jumps of the molecule between sites *q*,*f* and *p*,*g*.

The concentration dependences of the shear viscosity coefficients for the regular structure of sphero-cylinders D_s—D_c—L_c = 9—8—8 are shown in Fig. 8. The local coefficients for the presented site pairs (which are numbered by subscripts at the character η) refer to the surface regions of the sphere $\eta_{8,8}$ (curves *1*, *6*) (a part of curve *1* is shifted by four points to lower values) and the cylinder $\eta_{1,3}$ (curves *2*, *7*) and to the site pairs oriented along the connection line between the sphere and the cylinder: $\eta_{38,39}$ (curves *3*, *8*) at the center of the cylinder; $\eta_{41,42}$ (curves *4*, *9*), at the center of interconnection of the cylinder with the sphere; and $\eta_{45,45}$ (curves *5*, *10*), at the center of the sphere. With an increase in the filling of a porous system, the adsorbate viscosity increases. The coefficients markedly change with an increase in θ. Figure 8 demonstrates the important role of the surface potential of the walls and the temperature; as in Fig. 7, *b*, the regions of capillary condensation at a reduced temperature with two domes for the surface and central regions are shown.

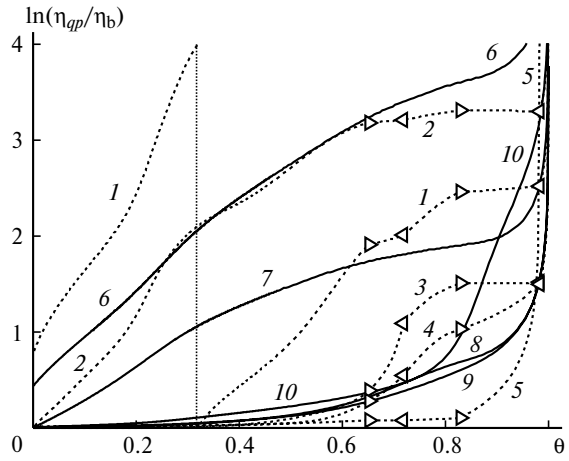

Fig. 8. Concentration dependences of the shear viscosity coefficients (η) for sphero-cylindrical structure with D_s—D_c—L_c = 9—8—8: $(\beta\varepsilon)^{-1} = 0.70$ (*1—5*), 1.23 (*6—10*); the following values are given: $\eta_{1,3}$ (*2*, *7*), $\eta_{8,8}$ (*1*, *6*), $\eta_{38,39}$ (*3*, *8*), $\eta_{41,42}$ (*4*, *9*), and $\eta_{45,45}$ (*5*, *10*).

* * *

Thus, we constructed for the first time the full curves for vapor—liquid phase separation for the adsorbate occurring in a polydisperse system of narrow cylindrical pores. In the case of strong attraction, layer-by-layer condensation of molecules takes place, giving rise to additional near-wall domes in the adsorbate phase separation curves. The number of these additional domes depends on the binding energy, the average characteristic pore size, and the proportion of the contributions of pores with the minimum size. When the pore size distribution is discrete, the overall dome corresponding to filling of the central sites is separated into a series of discrete (narrow) domes characterizing filling of the particular pores with different diameters. A similar splitting is manifested for surface domes due to different curvatures of pore walls and, as a consequence, different adsorbent—adsorbate interaction energies. The developed procedure reflects the effect of volume limitedness in the pores with different characteristic size.

The relationship between the spatial structures of the adsorption sites of different types and the multi-dome pattern of phase diagrams was demonstrated. Whereas under the action of the surface potential, the vapor—liquid coexistence curve for pores with a simple geometry is separated into several domes, in the case of complex porous systems, this curve should experience additional separation due to the difference in the characteristic sizes of the pores involved in the system (*i.e.*, the number of domes in pores with a simple geometry is minimum for a phase diagram of a complex porous system).

The curving of domes on the complete phase diagram of the system is due to the simultaneous filling of pores with different diameters (the domes for separate pores do not exhibit clear-cut curving) with a change in the overall degree of filling of a porous system at a fixed external pressure. Thus, even for a set of isolated pores, the pattern of phase diagram depends on the proportion of pores of different widths included in the system. The allowance for end effects on intersection of cylindrical pores of a finite length and the presence of sphero-cylindrical structure give rise to additional domes with respect to those in a polydisperse system of isolated pores. This is of crucial importance for the interpretation of experimental adsorption isotherms for micro- and mesoporous sorbents that exhibit adsorption hysteresis. In real adsorbents with continuous pore size distribution, the phase state of the adsorbate depends on the pore size in the given local areas of the adsorbent and in the surrounding areas. As a result, to calculate the phase distribution for the adsorbate, not only the pore size distribution should be known but also the functions characterizing the adsorbent structure.

The influence of characteristic pore dimensions on the conditions of existence of two-phase states was studied. The specific nature of narrow-pore systems was confirmed. It was found that a temperature below 60 K is needed to observe a two-phase state of nitrogen in micropores. This fact is in good agreement with numerous data on the absence of two-phase states at temperatures above 70 K.

The pattern of distribution of the vapor and liquid phases influences the local dynamic characteristics and changes their concentration dependences. The activation energies for the surface migration of molecules in narrow pores have a crucial influence on the temperature and concentration dependences of the self-diffusion and shear viscosity coefficients.

This work was financially supported for the Russian Foundation for Basic Research (Project No. 00-03-32153).

References

1. M. E. Fisher and H. Nakanishi, *J. Chem. Phys.*, 1981, **75**, 5857.
2. H. Nakanishi and M. E. Fisher, *J. Chem. Phys.*, 1983, **78**, 3279.
3. P. Tarasona, U. M. B. Marconi, and R. Evans, *Mol. Phys.*, 1987, **60**, 573.
4. A. de Kreizer, T. Michalski, and G. H. Findenegg, *Pure Appl. Chem.*, 1991, **63**, 1495.
5. Yu. K. Tovbin and E. V. Votyakov, *Langmuir*, 1993, **9**, 2652.
6. E. V. Votyakov and Yu. K. Tovbin, *Zh. Fiz. Khim.*, 1994, **68**, 287 [*Russ. J. Phys. Chem.*, 1994, **68**, No. 2 (Engl. Transl.)].
7. Yu. K. Tovbin, *Izv. Akad. Nauk, Ser. Khim.*, 2003, 827 [*Russ. Chem. Bull., Int. Ed.*, 2003, **52**, 869].
8. D. N. Breck, *Zeolite Molecular Sieves*, Wiley, New York, 1974.
9. N. Dufau, P. L. Llewellyn, C. Martin, J. P. Coulomb, and Y. Grillet, in *Fundamentals of Adsorption 6*, Elsevier, Paris, 1998, p. 63.
10. M. Grun, K. Schumacher, and K. Unger, in *Fundamentals of Adsorption 6*, Elsevier, Paris, 1998, p. 569.
11. Yu. K. Tovbin, *Teoriya fiziko-khimicheskikh protsessov na granitse gaz—tverdoe telo* [*Theory of Physikochemical Processes at a Gas—Solid Interface*], Nauka, Moscow, 1990, 288 pp. (in Russian).
12. Yu. K. Tovbin, *Zh. Fiz. Khim.*, 2003, **77**, No. 10 [*Russ. J. Phys. Chem.*, 2003, **77**, No. 10 (Engl. Transl.)].
13. T. L. Hill, *Statistical Mechanics. Principles and Selected Applications*, McGraw-Hill, New York, 1956.
14. E. V. Votyakov, Yu. K. Tovbin, J. M. D. MacElroy, and A. Roche, *Langmuir*, 1999, **15**, 5713.
15. A. M. Vishnyakov, E. M. Piotrovskaya, E. N. Brodskaya, E. V. Votyakov, and Yu. K. Tovbin, *Zh. Fiz. Khim.*, 2000, **74**, 501 [*Russ. J. Phys. Chem.*, 2000, **74**, No. 3 (Engl. Transl.)].
16. E. Ruckenstein, A. S. Vaidyanathan, and G. R. Youngquist, *Chem. Eng. Sci.*, 1971, **26**, 1305.
17. V. Sh. Mamleev, P. P. Zolotarev, and P. P. Gladyshev, *Neodnorodnost' sorbentov* [*Sorbent Inhomogeneity*], Nauka, Alma-Ata, 1989, 287 pp. (in Russian).
18. Yu. K. Tovbin and E. V. Votyakov, *Izv. Akad. Nauk, Ser. Khim.*, 2001, 48 [*Russ. Chem. Bull., Int. Ed.*, 2001, **50**, 50].
19. Yu. K. Tovbin and D. V. Yeremich, *Colloids and Surfaces, A*, 2002, **206**, 363.
20. L. D. Gelb, K. E. Gubbins, R. Radhakrishnan, and M. Sliwinska-Bartkowiak, *Rep. Prog. Phys.*, 1999, **62**, 1573.
21. A. R. Ubellohde, *The Molten State of Matter*, J. Wiley, London, 1978.
22. M. Thommes, R. Kohn, and M. Froba, *Appl. Surf. Sci.*, 2002, **196**, 239.
23. M. Thommes and M. Froba, *J. Phys. Chem.*, 2000, **104**, 7932.
24. Yu. K. Tovbin, *Dokl. Akad. Nauk SSSR*, 1990, **312**, 1425 [*Dokl. Chem.*, 1990 (Engl. Transl.)].
25. Yu. K. Tovbin, *Progr. Surf. Sci.*, 1990, **34**, 1.
26. Yu. K. Tovbin and N. F. Vasyutkin, *Izv. Akad. Nauk, Ser. Khim.*, 2001, 1496 [*Russ. Chem. Bull., Int. Ed.*, 2001, **50**, 1572].

Received April 21, 2003;
in revised form June 20, 2003